Science and Technology of Advanced Materials

ISSN: 1468-6996 (Print) 1878-5514 (Online) Journal homepage: www.tandfonline.com/journals/tsta20

Exploring partially reduced CeO(111) surface at the atomic scale using scanning probe microscopy

Kyungmin Kim, Masayuki Abe, Shigeki Kawai & Oscar Custance

To cite this article: Kyungmin Kim, Masayuki Abe, Shigeki Kawai & Oscar Custance (2025) Exploring partially reduced CeO(111) surface at the atomic scale using scanning probe microscopy, Science and Technology of Advanced Materials, 26:1, 2528596, DOI: 10.1080/14686996.2025.2528596

To link to this article: https://doi.org/10.1080/14686996.2025.2528596

Published online: 01 Aug 2025.

SCIENCE AND TECHNOLOGY OF ADVANCED MATERIALS
2025, VOL. 26, NO. 1, 2528596
https://doi.org/10.1080/14686996.2025.2528596

Exploring partially reduced CeO_2(111) surface at the atomic scale using scanning probe microscopy

Kyungmin Kim [a], Masayuki Abe [a], Shigeki Kawai [b] and Oscar Custance [b]

[a]Graduate School of Engineering Science, Osaka University, Toyonaka, Japan;
[b]Center for Basic Research on Materials, National Institute for Materials Science, Tsukuba, Japan

ABSTRACT

Cerium dioxide (CeO_2) is extensively studied due to its exceptional redox properties, which are closely related to oxygen vacancy formation and the associated charging of cerium atoms from Ce^{4+} to Ce^{3+}. These charged species play an important role in promoting active sites in CeO_2-based catalysts. The existence of Ce^{3+} atoms is typically characterized by means of surface spectroscopic techniques, because the direct atomic-scale observation and discrimination of Ce^{3+} ions from Ce^{4+} atoms remains challenging. Here, we use simultaneous scanning tunneling microscopy (STM) and atomic force microscopy (AFM) complemented by force spectroscopy to characterize candidates to Ce^{3+} atoms on partially reduced CeO_2(111) samples. While STM images reveal electronic modulations of the atomic contrast in the form of an inhomogeneous shading, AFM clearly differentiates these electronic features from the true topographic atomic structure. The chemical reactivity of these candidates to Ce^{3+} atoms is quantified against the Ce^{4+} counterparts by means of force spectroscopy using carbon monoxide functionalized probes. This study demonstrates that the combination of STM with AFM and force spectroscopy bears great potential to provide robust atomic-level insights into the chemistry of defects at ceria surfaces.

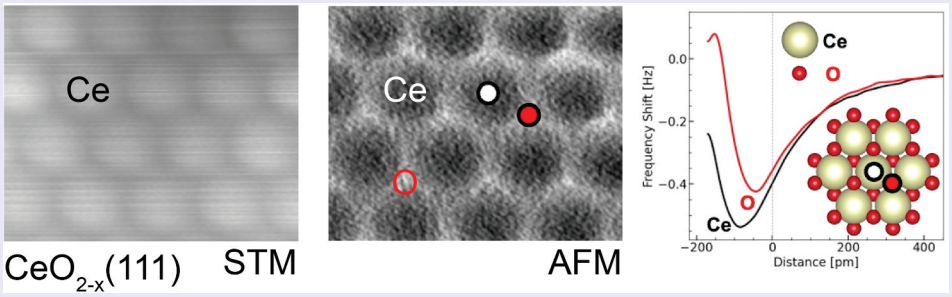

IMPACT STATEMENT

We directly visualize and chemically distinguish Ce, O, and defective Ce sites of the CeO_2(111) surface, as well as CO molecules on top of it, using high-resolution STM, AFM, and force spectroscopy with functionalized probes.

ARTICLE HISTORY
Received 5 May 2025
Revised 13 June 2025
Accepted 30 June 2025

KEYWORDS
Metal oxide surface; ceria; scanning tunneling microscopy; atomic force microscopy; force spectroscopy; Ce3+

1. Introduction

Cerium dioxide (CeO_2, ceria) is widely recognized for its exceptional redox properties, which stem from the reversible transition between Ce^{4+} and Ce^{3+} oxidation states. These properties enable efficient oxygen storage and release, making CeO_2 highly effective in various catalytic processes, including the water-gas shift reaction, carbon monoxide (CO) oxidation, and methane reforming [1–4]. Central to these redox processes is the formation of oxygen vacancies during ceria reduction, significantly influencing reaction pathways and catalytic performance. The generation of a single oxygen vacancy typically results in the simultaneous formation of two adjacent reduced Ce^{3+} ions [2].

Substantial research has been devoted to characterizing the formation, distribution, and behavior of these oxygen vacancies using surface-sensitive techniques such as scanning tunneling microscopy (STM), typically complemented by density functional theory (DFT) calculations [5–15], atomic force microscopy (AFM) [16,17], and X-ray photoelectron spectroscopy (XPS) [18–20]. Various methods have been developed over recent decades to engineer and control the formation of oxygen vacancies. Thermal reduction under

CONTACT Oscar Custance custance.oscar@nims.go.jp Center for Basic Research on Materials, National Institute for Materials Science, Tsukuba, Japan

ultra-high vacuum (UHV) conditions produces ordered vacancy structures predominantly at step edges and grain boundaries [5,9,11,13,14,16,17,21]. Chemical reduction methods using gases such as hydrogen, CO, or hydrocarbons selectively remove lattice oxygen atoms, forming water and carbon dioxide, and influencing the distribution of vacancies and Ce^{3+} sites [8,12,18]. Radiation-induced methods, such as electron-stimulated desorption (ESD), ion irradiation, and UV-light exposure, also provide precise control over vacancy generation and electron localization [19,20,22]. Jerratsch et al. [23] used ESD in combination with STM and DFT calculations to investigate the spatial correlation between oxygen vacancies and Ce^{3+} sites. Their results demonstrated that electrons released upon vacancy formation do not always localize on the immediate neighboring Ce ions but may instead occupy more distant sites. Achieving direct atomic-level identification and detailed characterization of Ce^{3+} remains challenging due to their subtle electronic and structural distinctions from Ce^{4+}, particularly when relying solely on STM [23].

Atomic-scale resolution STM and AFM offer powerful capabilities for elucidating local surface structures and chemistry. STM provides detailed insights into local electronic states, whereas AFM excels at direct atomic-scale structural imaging. Here, we combine STM and AFM to directly visualize cerium defects at CeO_2(111) thin-films grown on a copper substrate using probes functionalized on copper oxide areas adjacent to CeO_2 islands as well as probes functionalized with a CO molecule. The CuOx apexes produced on copper oxide areas exhibit stable covalent bonding configurations that usually expose an oxygen atom at the probe forefront [24], resulting in a rigid probe termination that enables force detection mainly via electrostatic interaction between the probe outermost oxygen atom and the surface atomic sites [25–28]. The flexibility of the CO functionalized probe can enhance small differences in the interaction force by the tilting effect of the molecule [29–32]. The rigidity of a CuOx apex, however, facilitates reaching the surface at closer distances. Force spectroscopy measurements [33,34] using these two types of probe terminations enabled us to differentiate the chemical reactivity of candidates to Ce^{3+} atoms relative to the Ce^{4+} sites. Our study provides a direct atomic-scale visualization of cerium defects, offering insights into their precise spatial distribution and chemical nature on the stable CeO_2(111) surface. These findings establish AFM as an essential complementary technique to STM, significantly enhancing atomic-scale characterization capabilities for metal oxide surfaces.

2. Experimental details

All experiments were conducted in an ultra-high vacuum (UHV) system (base pressure below 1×10^{-8} Pa) equipped with in-situ sample preparation tools and a home-built scanning probe microscope operated at 4.8 K using a commercial controller (Nanonis SPM Control System, SPECS, Germany).

The CeO_2(111) films were grown on a Cu(111) single crystal. The Cu(111) surface was initially cleaned by several cycles of Ar^+ sputtering and annealing, and then it was oxidized by exposing the sample to 1.0×10^{-5} Pa oxygen environment while keeping the substrate at 470 °C. The CeO_2(111) films were fabricated by depositing Ce (99.9%, GoodFellow, UK) on the oxidized Cu(111) surface in a 2.0×10^{-5} Pa oxygen environment, while annealing the sample at 485 °C. Upon deposition of Ce, the sample temperature was gradually reduced at a rate of ~1 °C/s in a 2.0×10^{-5} Pa oxygen environment until reaching 200 °C, at which point heating and oxygen flow ceased, and the crystal was left to cool down to room temperature under UHV conditions. For CeO_2 reduction, electron irradiation was performed by injecting 150 eV electrons (100 mC dose) incident on the surface at room temperature under UHV conditions. For experiments involving CO-functionalized probes, CO molecules were deposited on the CeO_2(111) surface by backfilling the UHV chamber and exposing the cold sample in the microscope to a total of 0.22 Langmuir of CO gas while keeping the sample temperatures below 23 K.

For both tunneling current detection and probe-surface interaction force measurements, we used the KolibriSensor (SPECS, Germany). The probe was initially sharpened *ex situ* to an apex radius of approximately 15 nm using a focused ion beam (DualBeam Helios5UX, ThermoFisher, USA), and subsequently conditioned *in situ* on copper oxide surface areas coexisting with the CeO_2 islands for atomic resolution imaging.

AFM experiments were performed in frequency modulation detection mode keeping constant the oscillation amplitude [35]. Image processing, analysis, and visualization were carried out using WSxM software [36].

3. Results and discussion

To investigate the structural and electronic characteristics of the partially reduced CeO_2(111) surface, we performed electron irradiation on the CeO_2(111) films [23]. Figure 1(a) presents an STM topographic image of the partially reduced CeO_2(111) surface. The moiré pattern observed in this STM image aligns with prior observations [7,8,10,12,15,37], and it arises from lattice mismatches and structural variations inherent in

the CeO_2(111) thin films [15,38]. Cross-sectional analysis, Figure 1(b), reveals step heights of approximately 0.31 nm (top to second terraces) and 0.34 nm (second to third terraces), closely matching previously reported experimental values as well as the theoretical crystallographic step height of 0.313 nm [39]. The slight decrease in step height observed with the increase of the film thickness likely results from an apparent increase of the tunneling barrier due to a reduced conductivity throughout the ceria thin-film.

The cross-section profile between points B' and C' indicates a subtle height difference of approximately 0.14 nm between the second terrace and the triangular feature apparent in Figure 1(a) (red square). Detailed topographic STM imaging of this triangular feature, Figure 1(c), reveals a distinct local contrasts, while constant-height AFM imaging in Figure 1(d) maintains consistent atomic resolution across the boundary between the terrace and the triangular structure without any topographic height difference. This observation suggests that the triangular contrast in STM does not have a structural origin but it rather seems to correspond to a variation in the film conductivity due to the accumulation of defects such as Ce^{3+} ions [2,40], subsurface oxygen vacancies [5], or interstitial defects [41].

To investigate the interplay between electronic and structural features observed on the partially reduced CeO_2(111) surface, simultaneous constant-height STM and AFM imaging over the same surface area at several bias voltages (Figure 2) were performed over a pristine surface area of the CeO_2(111) sample shown in Figure 1(a). At a positive sample bias of 1.2 V, Figure 2(a), the STM signal predominantly reveals the cerium atomic lattice, originating primarily from tunneling into Ce 4*f* states [23]. Conversely, at negative bias voltages, Figure 2(b), the STM contrast predominantly arises from the oxygen lattice [23,42]. The empty-states STM image exhibits a modulation of the atomic contrast by a mixture of triangular and hexagonal patterns, and the filled states STM image also displays localized areas of lower contrast; features that have been reported in other works [6,8,9,12–14,37]. The AFM images, in contrast, show a perfect hexagonal and homogeneous atomic pattern without any evidence of surface or subsurface defects for either polarities. The appearance of

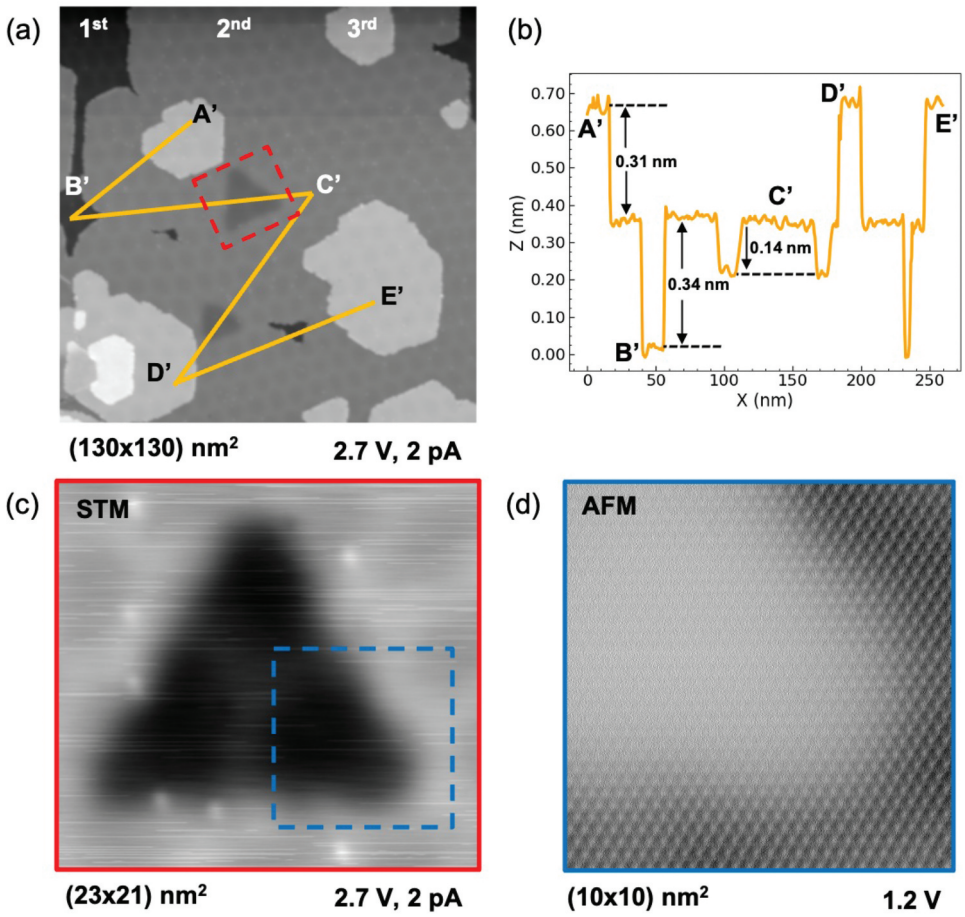

Figure 1. (a) Topographic STM image depicting a partially reduced CeO_2(111) thin film surface. (b) Height profile extracted from the cross-section marked in panel (a). (c) STM image of the region enclosed by a red square in panel (a), showing a sub-surface extended triangular formation due to electron irradiation. (d) Constant-height AFM image of the region indicated by a blue square in (c), demonstrating continuous atomic-scale resolution over the triangular formation. Experimental parameters: (a, c) bias voltage (*V*) was 2.7 V, tunneling current set point (*I*) was 2 pA; (d) *V* = 1.2 V; force sensor oscillation amplitude (*A*) was 60 pm, and force sensor free oscillation resonant frequency (f_0) was 989,098 Hz. Images measured with a CuOx-apex.

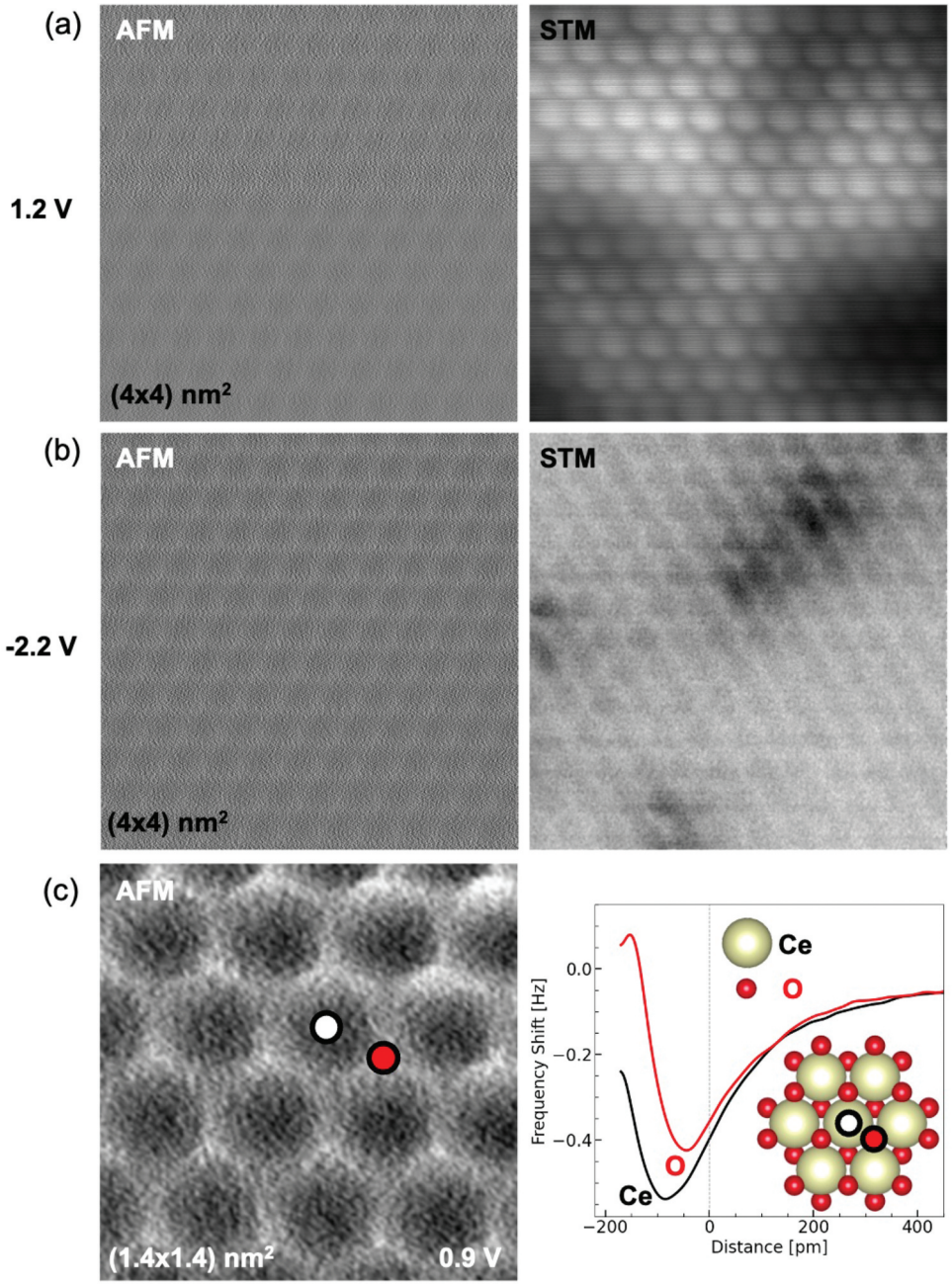

Figure 2. Simultaneously acquired constant-height STM and AFM images of a partially reduced $CeO_2(111)$ surface at different sample bias voltages: (a) 1.2 V probing empty electronic states dominated by cerium sites, and (b) −2.2 V probing filled electronic states highlighting oxygen sites. (c) Atomic resolution constant-height AFM image of a $CeO_2(111)$ surface with force spectroscopy curves obtained at representative atomic positions: Ce (black), O (red). Measurement points are indicated by color-coded dots, matching the Δf curves. The inset shows a surface model of the $CeO_2(111)$ lattice, indicating the atomic arrangement of Ce and O atoms. Experimental parameters: A = 60 pm, f_0 = 989098 Hz. (c) Data acquired with a CuOx-apex.

modulation in the STM signal in the absence of apparent defects near the surface evidences a complex relationship between the local electronic states and atomic structures buried well below the surface.

The modulations described in the empty-states STM image of Figure 2(a) seem to have a different origin than the extended triangular features shown in Figure 1(c); which are resolved by both STM and AFM. These triangular features have been observed upon reduction of $CeO_2(111)$ films by electron irradiation. The fact that they appear in the AFM image as an extended background with a wide boundary superimposed to the atomic structure points towards an electrostatic nature due to charge accumulation inside the film rather than to a local variation of the electronic structure by the presence of detects.

From the comparison of the simultaneous constant-height STM and AFM images, Figure 2(a), we can assign the atomic site with a dim contrast in the AFM images to the cerium atoms, as in empty-states STM images only the cerium atoms are resolved [23]. Similarly, we can differentiate the oxygen site from the

coordination vacancy position by juxtaposing with the filled-states image, which provide highest STM contrast over the topmost oxygen atoms [23]. However, atomic contrast in constant-height AFM imaging on heterogeneous surfaces significantly depends on the relative chemical interactions between the different atomic species and the probe apex atom, as well as on the probe-surface separation distance used during image acquisition. To corroborate our STM-based atomic identification and clarify the contrast in our AFM images, we conducted force spectroscopy measurements as it is illustrated in Figure 2(c). Δf curves were acquired over the cerium and oxygen atoms indicated by white and red dots, respectively, by bringing the probe towards the surface from the imaging separation distance and retracting it back until recovering the free-oscillation regime of the force sensor. Thus, the origin in the distance axis represents the separation at which the constant-height AFM image in Figure 2(c) was acquired. This separation distance closely matches the probe-surface separation used for imaging in Figures 2(a),(b) and the corresponding AFM signal values confirm that both cerium and oxygen atoms exert attractive interactions with the probe at this imaging distance. Taking into account that we measure with a CuOx-apex [27] likely to display an oxygen atom at the forefront [24], these Δf curves reveal a stronger attraction over the cerium site and a weaker interaction over the oxygen atom; features which are consistent with our hypothesis of an oxygen-terminated probe as well as with the initial atomic species assignment based on STM data. Thus, this combination of force spectroscopy and bias-dependent STM imaging enables us to establish a reliable identification of the Ce and O atomic sites. We will use the specific force signatures of these atoms for subsequent identification of atomic species at the CeO_2(111) surface, as long as the probe is terminated in an oxygen atom.

It is well established that Ce^{3+} sites generally emerge alongside oxygen vacancy formation during the reduction of ceria surfaces [2]. Previous DFT and transmission electron microscopy studies indicated that Ce^{3+} species predominantly reside on the surfaces of ceria nanoclusters [43], and during particle growth, ceria reduction typically remains confined to a thin surface region [44]. However, direct atomic-level identification of Ce^{3+} species has traditionally been challenging due to subtle electronic and structural differences compared to the Ce^{4+} sites [23].

Our study of partially reduced CeO_2(111) surfaces at the atomic scale reveals that not all the cerium atoms of the second atomic layer are equivalent. This is apparent in the simultaneous constant-height STM and AFM images displayed in Figure 3, which were measured with a bias voltage of 1.2 V. Consistently with the observations in Figure 2, the STM image displays a modulation of the atomic contrast, whereas the AFM image clearly resolves the atomic positions of the Ce and O atomic lattices. In the AFM image, a more attractive interaction force over some of the Ce sites — which appear enlarged and with a slightly darker contrast than the rest of the Ce atoms (see the white arrows) – is clear. Cross-sectional analysis of the AFM signal across these defective Ce atoms reveals an average of 21% stronger attractive interaction relative to regular Ce sites (including probe asymmetries, see Figure S1). This value is consistent with the outcome of our DFT calculations that predict a stronger interaction force over Ce^{3+} atoms with respect to the Ce^{4+}

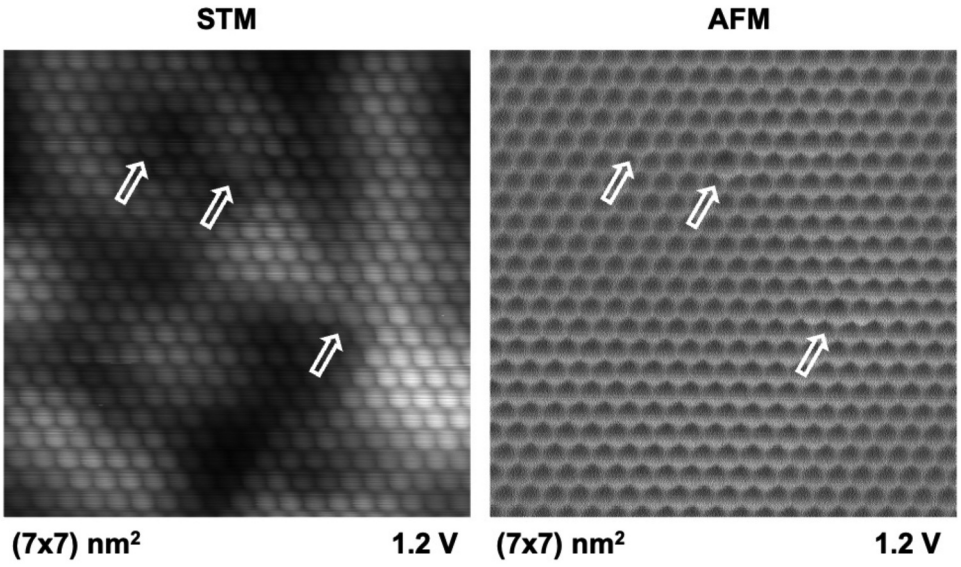

Figure 3. Constant-height STM and AFM images acquired simultaneously at a bias voltage of 1.2 V. Positions of defective Ce atoms candidates to Ce^{3+} are marked by white arrows. Experimental parameters: A = 60 pm, f_0 = 989098 Hz. Images obtained with a CuOx-apex.

counterparts when probing both species with an oxygen terminated probe [45]. These defective Ce atoms are therefore candidates to Ce^{3+}.

We have also characterized the interaction force over these defective Ce atoms using a CO-functionalized probe [29]. For this purpose, we deposited CO molecules on a partially reduced $CeO_2(111)$ surface at a very low coverage. Figure 4 presents an STM topography and a constant-height AFM image of a $CeO_2(111)$ terrace with a low coverage of CO molecules adsorbed on it. The topographic STM image reveals faint contrast, presenting the CO molecules as bright protrusions primarily populating the step edges. The AFM image of the same terrace resolves the protrusions detected by the STM as small clusters of CO molecules adsorbed mainly at the upper terrace of the step edge and unveils the presence of a considerable less number of CO molecules populating the terrace's inland. For the AFM probe functionalization, a CO molecule was picked up from the step [29], as this adsorption site shows more stability than the one at the inner part of the terrace, where CO molecules can laterally move easily due to the interaction with the probe.

Atomic-resolution AFM imaging and force spectroscopy measurements performed with a CO-functionalized probe are summarized in Figure 5. To preserve the probe integrity during imaging, the constant-height AFM image displayed in Figure 5(a) was acquired at a relatively larger probe-surface separation than the typical imaging conditions explored when using CuOx-terminated probes, resulting in a lower AFM contrast between Ce and O species yet maintaining sufficient resolution to differentiate between the atomic sites. A hexagonal lattice representing the $CeO_2(111)$ structure has been superimposed to the AFM image to highlight the position of the Ce atoms. Cyan, blue, and purple dots indicate defective Ce atoms that exhibit a more attractive AFM signal, similar to those observed in Figure 3, confirming their distinct chemical reactivity compared to Ce^{4+} sites. Orange and yellow dots denote nearest Ce neighbors to the defective Ce site.

Figure 5(b) presents force spectroscopy curves acquired at each corresponding color-coded site appearing in Figure 5(a). The Δf curves obtained at the defective Ce sites (cyan, blue, purple) and the reference Ce^{4+} site (black) show a comparable maximum attractive interaction occurring at nearly identical probe-surface distances; however, distinct variations appear in the magnitude of the minima. Furthermore, comparison of the magnitudes of the minima indicates an increased attractive interaction of 11.6% (cyan), 17.0% (blue), and 22.6% (purple) relative to the reference Ce^{4+} site. Variations in the magnitude of the interaction minima among defective Ce sites may reflect subtle differences in the subsurface local chemical environments, likely due to the presence of subsurface oxygen vacancies or interstitials. For the nearest-neighbor sites to a defective Ce atom (orange and yellow), the Δf curves exhibit nearly identical interaction, characterized by minima shifted by 10 pm relative to the Ce^{4+} reference site, and an increased attractive interaction of approximately 3.5%.

In conclusion, our combined STM and AFM approach provides comprehensive insights into the atomic-scale structural and electronic characteristics of partially reduced $CeO_2(111)$ surfaces. STM effectively visualizes subtle electronic features, such as modulation of the atomic contrast in the form of combined triangular and hexagonal shading, arising

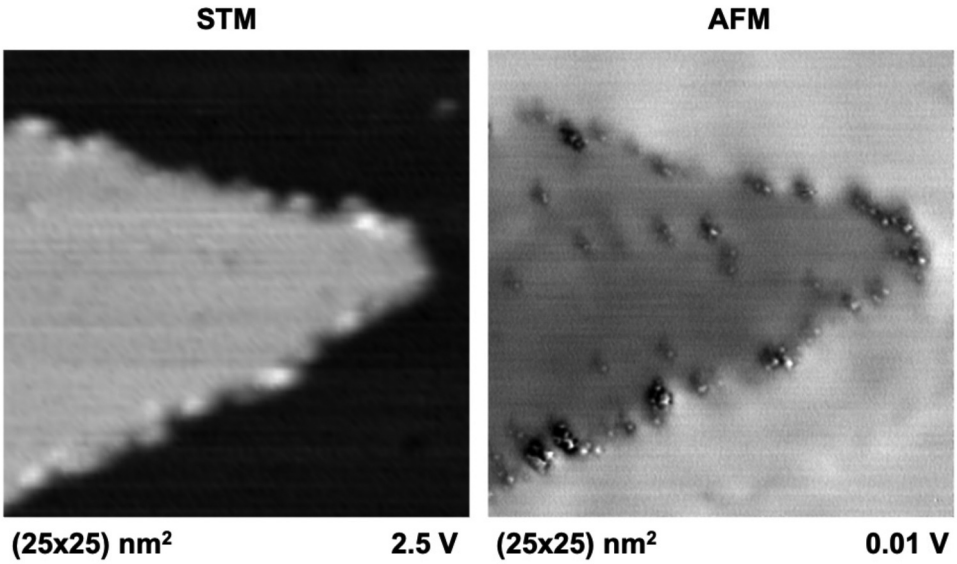

Figure 4. Topographic STM and constant-height AFM images of a CeO_2 island with adsorbed CO molecules predominantly located at the upper terrace of the step edge. Experimental parameters: A = 60 pm and f_0 = 992467 Hz. Images measured with a CuOx-apex.

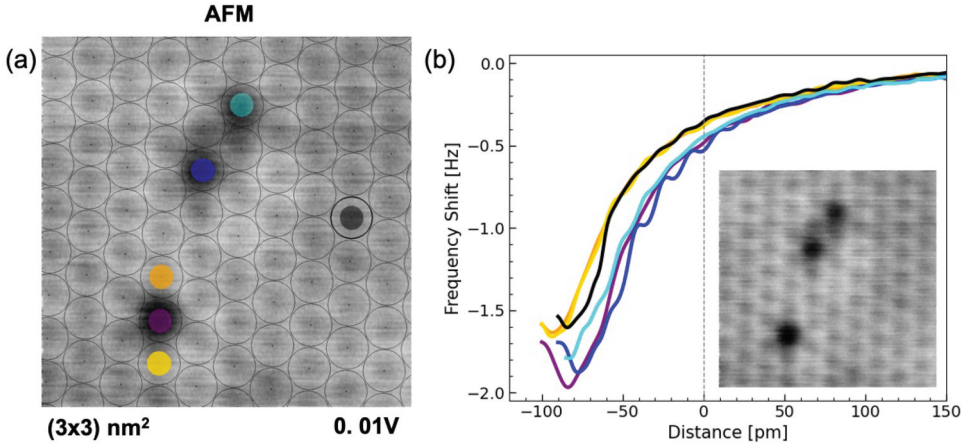

Figure 5. (a) Constant-height AFM image measured using a CO-functionalized probe with a hexagonal lattice superimposed to highlight the cerium sites. (b) Force spectroscopy curves measured at the center of each color-coded dot in (a) with a CO molecule at the probe apex. The inset presents the raw AFM image displayed in (a). Experimental parameters: $V = 0.01$ V, $A = 60$ pm, $f_0 = 992467$ Hz.

primarily from local variations in the film conductivity possibly linked to buried defects such as Ce^{3+} ions, subsurface oxygen vacancies, or interstitials. Complementarily, AFM delivers precise structural information at the atomic scale of the outermost surface layers, independently of the local variations of the film conductivity. The combination of bias-dependent constant height STM imaging and force spectroscopy enabled the identification of the cerium and oxygen atomic sites. The direct visualization and force-spectroscopy based chemical characterization of candidates to Ce^{3+} sites populating the outermost Ce atomic layer is presented, allowing us to cast new light on the subtle structural and electronic differences with the Ce^{4+} sites. This study shows that the combination of simultaneous STM and AFM imaging with force spectroscopy measurements can be a strong method to enhance atomic-level understanding of defect chemistry in ceria surfaces.

Acknowledgments

OC is grateful to M. González-Lastre, E. Fernandez-Villanueva, P. Pou, M. V. Ganduglia-Pirovano, and R. Perez for enlightening discussions about ceria surfaces. KK thanks D. Katsube for insightful discussions and acknowledges the support from the Program for Leading Graduate Schools: "Interactive Materials Science Cadet Program."

Disclosure statement

No potential conflict of interest was reported by the author(s).

Funding

This work was supported by The National Institute for Materials Science (NIMS) grants [AG2030 and AM2100], by The Ministry of Education, Culture, Sports, Science and Technology of Japan (MEXT) through several Grant-in-Aid for Scientific Research [19H05789, 21H01812, 21K18876, 22H00285, 24K01350, 24K21716], and by the JSPS DC1 fellowship for young researchers 23KJ1516 (KK).

ORCID

Kyungmin Kim http://orcid.org/0000-0002-3147-5100
Masayuki Abe http://orcid.org/0000-0001-5619-3911
Shigeki Kawai http://orcid.org/0000-0003-2128-0120
Oscar Custance http://orcid.org/0000-0001-7931-603X

References

[1] Trovarelli A. Catalysis by ceria and related materials. London: Imperial College Press; 2002.
[2] Skorodumova NV, Simak SI, Lundqvist BI, et al. Quantum origin of the oxygen storage capability of ceria. Phys Rev Lett. 2002;89(16):166601. doi: 10.1103/PhysRevLett.89.166601
[3] Vayssilov GN, Lykhach Y, Migani A, et al. Support nanostructure boosts oxygen transfer to catalytically active platinum nanoparticles. Nat Mater. 2011;10(4):310–315. doi: 10.1038/nmat2976
[4] Ma Y, Gao W, Zhang Z, et al. Regulating the surface of nanoceria and its applications in heterogeneous catalysis. Surf Sci Rep. 2018;73(1):1–36. doi: 10.1016/j.surfrep.2018.02.001
[5] Esch F, Fabris S, Zhou L, et al. Electron localization determines defect formation on ceria substrates. Science. 2005;309(5735):752–755. doi: 10.1126/science.1111568
[6] Naya K, Ishikawa R, Fukui K. Oxygen-vacancy-stabilized positively charged Au nanoparticles on CeO_2 (111) studied by reflection–absorption infrared spectroscopy. J Phys Chem C. 2009;113(24):10726–10730. doi: 10.1021/jp902564w
[7] Dvořák F, Stetsovych O, Steger M, et al. Adjusting morphology and surface reduction of CeO_2 (111) thin films on cu(111). J Phys Chem C. 2011;115(15):7496–7503. doi: 10.1021/jp1121646
[8] Yang F, Graciani J, Evans J, et al. CO oxidation on inverse CeO_x /Cu(111) catalysts: high catalytic

activity and ceria-promoted dissociation of O_2. J Am Chem Soc. 2011;133(9):3444–3451. doi: 10.1021/ja1087979

[9] Pan Y, Nilius N, Freund HJ, et al. Titration of Ce3+ ions in the CeO_2 (111) surface by Au adatoms. Phys Rev Lett. 2013;111(20):206101. doi: 10.1103/PhysRevLett.111.206101

[10] Hasegawa T, Shahed SMF, Sainoo Y, et al. Epitaxial growth of CeO_2 (111) film on Ru(0001): scanning tunneling microscopy (STM) and x-ray photoemission spectroscopy (XPS) study. J Chem Phys. 2014;140(4):044711. doi: 10.1063/1.4849595

[11] Luches P, Pagliuca F, Valeri S. Structural and morphological modifications of thermally reduced cerium oxide ultrathin epitaxial films on Pt(111). Phys Chem Chem Phys. 2014;16(35):18848–18857. doi: 10.1039/C4CP02723J

[12] Shahed SMF, Hasegawa T, Sainoo Y, et al. Stm and xps study of CeO_2 (111) reduction by atomic hydrogen. Surf Sci. 2014;628:30–35. doi: 10.1016/j.susc.2014.05.008

[13] Lustemberg PG, Pan Y, Shaw BJ, et al. Diffusion barriers block defect occupation on reduced CeO_2 (111). Phys Rev Lett. 2016;116(23):236101. doi: 10.1103/PhysRevLett.116.236101

[14] Tovt A, Stetsovych V, Dvořák F, et al. Ordered phases of reduced ceria as inverse model catalysts. Appl Surf Sci. 2019;465:557–563. doi: 10.1016/j.apsusc.2018.09.068

[15] Yi Z, Fan Y, Xinhe B. Growth and structures of monolayer and bilayer CeO_x nanostructures on Au (111). Surf Sci. 2019;679:31–36. doi: 10.1016/j.susc.2018.08.017

[16] Torbrügge S, Reichling M, Ishiyama A, et al. Evidence of subsurface oxygen vacancy ordering on reduced CeO_2 (111). Phys Rev Lett. 2007;99(5):056101. doi: 10.1103/PhysRevLett.99.056101

[17] Olbrich R, Murgida GE, Ferrari V, et al. Surface stabilizes ceria in unexpected stoichiometry. J Phys Chem C. 2017;121(12):6844–6851. doi: 10.1021/acs.jpcc.7b00956

[18] Mullins DR, Robbins MD, Zhou J. Adsorption and reaction of methanol on thin-film cerium oxide. Surf Sci. 2006;600(7):1547–1558. doi: 10.1016/j.susc.2006.02.011

[19] Kumar A, Devanathan R, Shutthanandan V, et al. Radiation-induced reduction of ceria in single and polycrystalline thin films. J Phys Chem C. 2012;116(1):361–366. doi: 10.1021/jp209345w

[20] Wang GD, Kong DD, Pan YH, et al. Low energy Ar-ion bombardment effects on the CeO_2 surface. Appl Surf Sci. 2012;258(6):2057–2061. doi: 10.1016/j.apsusc.2011.04.103

[21] Rong W, Chen H, Huang Z, et al. Strain-induced oxygen vacancies in monolayered CeO_2 (111) islands grown on Pt(111). J Phys Chem C. 2020;124(11):6284–6289. doi: 10.1021/acs.jpcc.0c00630

[22] Wu TS, Syu LY, Lin CN, et al. Enhancement of catalytic activity by UV-light irradiation in CeO_2 nanocrystals. Sci Rep. 2019;9(1):8018. doi: 10.1038/s41598-019-44543-2

[23] Jerratsch JF, Shao X, Nilius N, et al. Electron localization in partially reduced ceria films: a study with scanning-tunneling microscopy and density-functional theory. Phys Rev Lett. 2011;106(24):246801. doi: 10.1103/PhysRevLett.106.246801

[24] Mönig H, Hermoso DR, Díaz Arado O, et al. Submolecular imaging by noncontact atomic force microscopy with an oxygen atom rigidly connected to a metallic probe. ACS Nano. 2016;10(1):1201–1209. doi: 10.1021/acsnano.5b06513

[25] Mönig H, Amirjalayer S, Timmer A, et al. Quantitative assessment of intermolecular interactions by atomic force microscopy imaging using copper oxide tips. Nat Nanotechnol. 2018;13(5):371–375. doi: 10.1038/s41565-018-0104-4

[26] Liebig A, Giessibl FJ. In-situ characterization of o-terminated cu tips for high-resolution atomic force microscopy. Appl Phys Lett. 2019;114(14):143103. doi: 10.1063/1.5085747

[27] Wiesener P, Förster S, Merkel M, et al. Standardization of chemically selective atomic force microscopy for metal oxide surfaces. ACS Nano. 2024;18(33):14315–14325. doi: 10.1021/acsnano.4c03155

[28] Schulze LB, Yesilpinar D, Timmer A, et al. Benchmarking atomically defined AFM tips for chemical-selective imaging. Nanoscale. 2021;13(32):13617–13623. doi: 10.1039/D1NR04080D

[29] Gross L, Mohn F, Moll N, et al. The chemical structure of a molecule resolved by atomic force microscopy. Science. 2009;325(5944):1110–1114. doi: 10.1126/science.1176210

[30] Moll N, Gross L, Mohn F, et al. The mechanisms underlying the enhanced resolution of atomic force microscopy with functionalized tips. New J Phys. 2010;12(12):125020. doi: 10.1088/1367-2630/12/12/125020

[31] Hämäläinen SK, van der Heijden N, van der Lit J, et al. Intermolecular contrast in atomic force microscopy images without intermolecular bonds. Phys Rev Lett. 2014;113(18):186102. doi: 10.1103/PhysRevLett.113.186102

[32] Néel N, Kröger J. Atomic force extrema induced by the bending of a CO-functionalized probe. Nano Lett. 2021;21(5):2318–2323. doi: 10.1021/acs.nanolett.1c00268

[33] Lantz MA, Hug HJ, Hoffmann R, et al. Quantitative measurement of short-range chemical bonding forces. Science. 2001 Mar;291(5513):2580–2583. doi: 10.1126/science.1057824

[34] Sugimoto Y, Pou P, Abe M, et al. Chemical identification of individual surface atoms by atomic force microscopy. Nature. 2007 Mar;446(7131):64–67. doi: 10.1038/nature05530

[35] Albrecht TR, Grütter P, Horne D, et al. Frequency modulation detection using high-q cantilevers for enhanced force microscope sensitivity. J Appl Phys. 1991;69(2):668–673. doi: 10.1063/1.347347

[36] Horcas I, Fernández R, Gómez-Rodríguez JM, et al. WSxM: a software for scanning probe microscopy and a tool for nanotechnology. Rev Sci Instrum. 2007;78(1):013705. doi: 10.1063/1.2432410

[37] Shao W, Zhang Y, Zhou Z, et al. Dynamic control and quantification of active sites on ceria for CO activation and hydrogenation. Nat Commun. 2024;15(1):9620. doi: 10.1038/s41467-024-53948-1

[38] Stetsovych O, Dvořák F, Szabová L, et al. Nanometer-range strain distribution in layered incommensurate systems. Phys Rev Lett. 2012 Dec;109(26):266102. doi: 10.1103/PhysRevLett.109.266102

[39] Nörenberg H, Briggs GAD. Surface structure of CeO_2 (111) studied by low current STM and electron

diffraction. Surf Sci. 1998;402–404:734–737. doi: 10.1016/S0039-6028(97)00999-0

[40] Choudhury B, Chetri P, Choudhury A. Oxygen defects and formation of Ce^{3+} affecting the photocatalytic performance of CeO_2 nanoparticles. RSC Adv. 2014;4(9):4663–4671. doi: 10.1039/C3RA44603D

[41] Yasunaga K, Yasuda K, Matsumura S, et al. Electron energy-dependent formation of dislocation loops in CeO_2. Nucl Instrum Methods Phys Res B. 2008;266 (12–13):2877–2881. doi: 10.1016/j.nimb.2008.03.204

[42] Wolf MJ, Castleton CWM, Hermansson K, et al. STM images of anionic defects at CeO_2(111)—a theoretical perspective. Front Chem. 2019;7:212. doi: 10.3389/fchem.2019.00212

[43] Loschen C, Bromley ST, Neyman KM, et al. Understanding ceria nanoparticles from first-principles calculations. J Phys Chem C. 2007;111(28):10142–10145. doi: 10.1021/jp072787m

[44] Wu L, Wiesmann HJ, Moodenbaugh AR, et al. Oxidation state and lattice expansion of CeO_{2-x} nanoparticles as a function of particle size. Phys Rev B. 2004;69 (12):125415. doi: 10.1103/PhysRevB.69.125415

[45] Custance O, González-Lastre M, Kim K, et al. Submitted.